Facet-Dependent Adsorption of Rare Earth Elements (REEs) and Actinides onto Goethite: REE Pattern Variability and Cerium Anomaly

Muqeet Iqbal, Keran Zhang, Mélanie Davranche, Aline Dia, Lionel Dutruch, Delphine Vantelon, Gildas Ratié, Benoit Maxit, Khalil Hanna, Rémi Marsac

Facet dependent adsorption of rare earth elements (REE) and actinides onto goethite: REE pattern variability and cerium anomaly

MUQEET IQBAL[1,6], KERAN ZHANG[2], MÉLANIE DAVRANCHE[1], ALINE DIA[1], LIONEL DUTRUCH[1], DELPHINE VANTELON[3], GILDAS RATIÉ[4], BENOIT MAXIT[5], KHALIL HANNA[6], AND RÉMI MARSAC[7]*

[1]Univ Rennes, CNRS, Géosciences Rennes, UMR 6118, 35000 Rennes, France

[2]Critical Metals for Enabling Technologies, School of Science, Constructor University, Campus Ring 1, 28759, Bremen, Germany

[3]Synchrotron SOLEIL, L'ormes des Merisiers, Départementale 128, 91190 Saint Aubin, France

[4]Nantes Université, Univ. Angers, Le Mans Université, CNRS, Laboratoire de Planétologie et Géosciences LPG UMR 6112, F-44000 Nantes, France

[5]Cordouan Technologies, Av. Canteranne, 33600 Pessac, France

[6]Univ Rennes, Ecole Nationale Supérieure de Chimie de Rennes, CNRS, ISCR-UMR 6226, F-35000, Rennes, France

[7] Université Paris Cité, Institut de physique du globe de Paris, CNRS, F-75005 Paris, France

(*correspondence: remi.marsac@cnrs.fr)

Abstract. Assessing the fate of contaminants in the environment requires a deep understanding of intrinsic adsorption mechanisms on natural minerals, such as Fe-oxyhydroxides. In this study, we proposed an innovative approach to probe site heterogeneities on the goethite surface by comparing the adsorption behavior of rare earth elements (REE; including Sc, Y and all lanthanides; Ln) except Pm, as well as Th and U. A surface loading-dependent adsorption of Ln and Y was observed, with a shift from (i) preferential middle to heavy REE adsorption, and (ii) limited to substantial fractionation between Y and Ho as the loading increased. These observations are likely attributable to the formation of strong and weak complexes onto the (021) and (110)/(100) goethite faces, at low and high loading, respectively. Additionally, Ce-anomaly, characteristic of Ce(III) partial oxidation to Ce(IV), was only observed at high loading. By drawing analogy with Th(IV) and Sc(III), Ce(IV) is expected to outcompete Ln(III) and Y adsorption and stabilize primarily at the strong sites on the (021) face, even under conditions of high loading. The outcome of this study, supported by charge distribution-multi site complexation (CD-MUSIC) calculation, provides new insights into the impact of facet-dependent adsorption and redox processes on Fe-oxyhydroxides.

Keywords: Fe(III) oxy(hydr)oxide; surface complexation; rare earth elements patterns; Ce oxidation; actinides

Synopsis: This study uses rare earth elements to probe facet-dependent surface complexation and redox processes onto goethite, which affects the environmental fate of many contaminants.

38 **Graphical abstract**

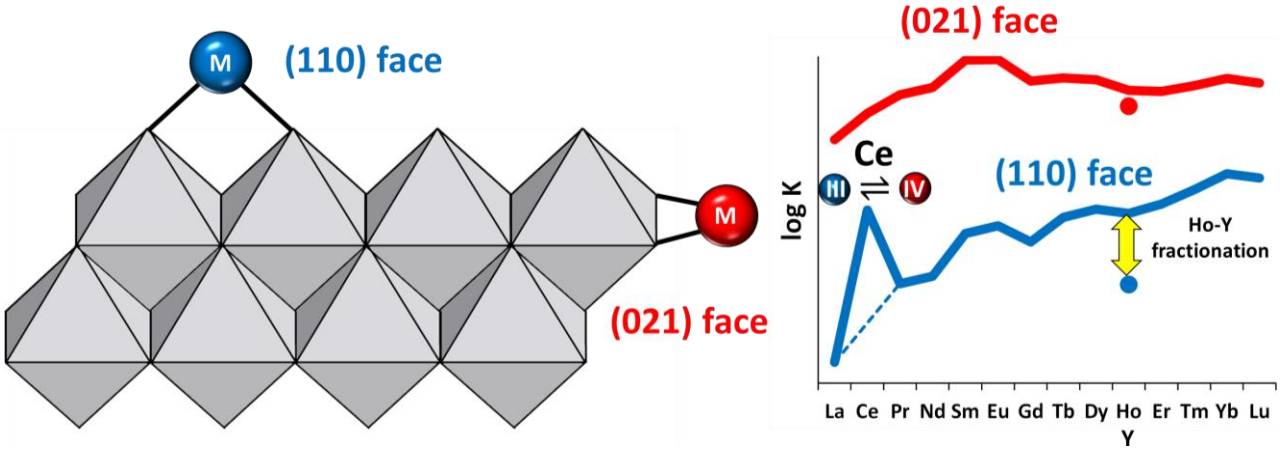

39
40

1. Introduction

Iron oxyhydroxides are widely present in the environment with different composition, mineralogy and morphology,[1] and play a key role in the speciation, bioavailability and transport of the contaminants.[2–4] They exhibit distinct crystal faces with different binding sites, leading to different adsorption mechanisms.[5–8] For instance, the facet dependent adsorption on goethite is generally attributed to the formation of strong bidentate complexes between metal ions and two adjacent ≡FeO groups at the edge of the same Fe(III) octahedra (or mononuclear edge sharing complex) of the (021) face (group *Pbnm*), or weaker ones at the corners of two distinct Fe(III) octahedra (binuclear corner sharing complex) at the (110)/(100) faces (**Figure 1**).[9–13] To determine facet-controlled adsorption, characterization of particle morphology and reactivity is necessary using a combination of solid-state techniques (e.g. transmission electron microscopy (TEM), X-ray diffraction (XRD), atomic force microscopy (AFM),[7,8]) and aqueous phase measurements. However, accurate particle characterization in polydisperse nanoparticle suspensions, which exhibit diverse surface and crystallographic properties, remains a challenging task.[14,15] Therefore, it is important to develop new approaches to probe surface site densities and heterogeneities in aqueous suspensions, and subsequently incorporate facet-dependent adsorption processes into environmental speciation models.

Rare earth elements (REE; including Sc, Y and all lanthanides (Ln) except Pm) are mainly trivalent in environmentally relevant conditions and form a highly coherent series of naturally occurring elements, whose chemical properties vary regularly along the series due to subtle differences in their chemical behavior, except Sc with its smaller ionic radius. They are now considered as emerging contaminants as a result of their growing demand in modern technologies,[16,17] their increased concentrations in several environmental compartments (rivers,

lakes, groundwaters, and coastal seawater)[18] and their ecological risks.[19,20] They have also been studied for a long time as tracers of different hydro-biogeochemical processes in present and ancient environments.[21–23] Their relative affinity for reactive sites can be visualized in the plot of the intrinsic stability constants ($\log_{10}$ K), or the partition coefficient between two phases ($\log_{10}$ K_d) versus the REE atomic number. For instance, different and specific shapes of REE $\log_{10}$ K patterns can emerge based on the sorbent or ligand used. A change in the REE pattern could be directly attributed to the changes in REE species formed at heterogeneous surfaces like quartz,[24] iron hydroxides,[25] manganese oxides,[26] clay minerals,[27] bacterial cells,[28,29] algae,[30] nanoplastics,[31] or natural organic colloids.[32,33] Moreover, the presence of the so-called tetrad effect (i.e. visualized as "waves" in the REE pattern), which arises from spin-orbit coupling of the f-electrons, serves as an indicator of inner-sphere complexation.[34,35] Additionally, Ce(III) can be oxidized to Ce(IV)[36,37] in low temperature environments, and the preferential scavenging of Ce(IV) compared to Ce(III) can give rise to the development of so-called Ce anomaly within REE patterns. The presence or the absence of a Ce anomaly in natural samples is widely used as a proxy of (paleo)redox conditions.[21,36,38] However, the mechanisms driving the oxidation of Ce(III) to Ce(IV) at mineral surfaces remain elusive.

In this study, REE were used to probe diverse facet-dependent processes on goethite, one of the most abundant and thermodynamically stable iron oxyhydroxides.[1] 100-150nm long needle-shaped goethite particles were chosen for their well-characterized surface structure, facet-dependent site density and surface reactivity with various ions.[6–8,10] Additionally, we explored the binding behavior of U, and Th, which may naturally co-occur and compete with REE in many environmental settings.[39] Examining the adsorption of these cations alongside REE may provide valuable insights into binding mechanisms and Ce-anomalies.[24,40] Batch experiments

were conducted from pH 3 to 7 and concentrations of all REE, Th, and U, in multi-metal ion systems. The experimental data were complemented by employing the Charge Distribution-Multi Site Complexation model (CD-MUSIC) for mechanistic surface complexation modeling. We discussed the impact of specific crystal facets of goethite on adsorption processes, thereby influencing the mobility of REE and the redox speciation of Ce. This approach serves as a robust tool for predicting the speciation of REE, Th, and U in the environment.

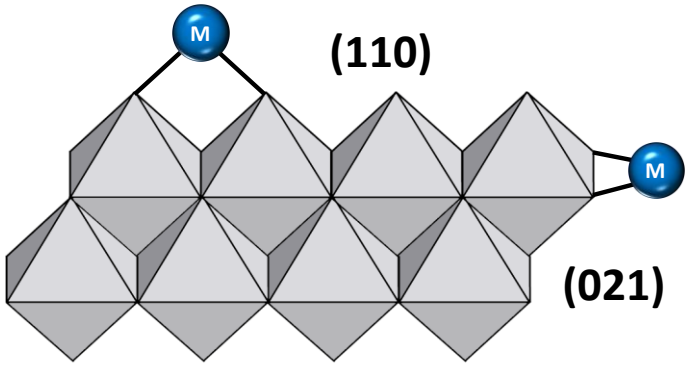

Figure 1. Goethite morphology and surface complexes proposed for metal ions at the (110) (bidentate corner sharing, weak complex) and (021) (bidentate edge sharing, strong complex) crystallographic faces (group *Pbnm*).[9–13]

2. Materials and Methods

Materials used are described in Supporting Information (Appendix A).

Synthesis and characterization of goethite particles. The presently used goethite batch was synthesized and characterized in a previous study,[41] and followed previously described procedure.[7,8,42] More details are provided in SI (Appendix B). The BET specific surface area (SSA) was 81 ± 1 m^2 g^{-1}, and the isoelectric point (IEP) of goethite was found equal to 9.1 using a zeta-potential analyzer (NanoBrook 90Plus zeta, Brookhaven, USA). The purity of goethite was confirmed by X-ray diffraction (XRD) and goethite nanoparticles were characterized by

transmission electron microscopy (LVEM5-TEM) (**Figure S1**), which confirmed that goethite has a typical needle-like shape, with length between 110 and 150 nm and width of 8−12 nm.

Batch experiments. The batch sorption experiments were carried out in opaque 250 mL HDPE reactors at room temperature (20°C ± 2) under ambient (air) conditions. The experiments were conducted in a 100 mL of a solution containing all Ln except Pm, as well as Sc, Y, Th, and U simultaneously in 5 mM NaCl as a background electrolyte with 0.1 g L^{-1} of goethite suspension. Batch experiments were initiated at low pH, due to the use of 5% v/v nitric acid stock solution containing REE, Th and U. Following pH adjustment, using HCl or NaOH (0.1 M), solutions were shaken in an oscillating table for 24 h, then the final pH was measured, and the samples were subsequently filtered through 0.2 μm (Sartorius® PES filters) for concentration determination. 24h equilibration was considered enough to reach a steady-state based on kinetic experiments summarized in the SI (**Figure S2**, Appendix C). Three sets of pH sorption edge experiments were conducted in the pH range 3 to 7 for total metal ion concentrations ([M]) of 1×10^{-7} M, 7×10^{-7} M, and 7×10^{-6} M. The adsorption isotherm experiments were carried out at pH 5.5 ± 0.1, by adjusting it several times during the reaction, for [M] ranging from 10^{-7} M to 10^{-5} M.

All REE, Th, and U and Fe concentrations in solution were measured using a Quadrupole ICP-MS (Agilent Technologies 7700×) following the procedures detailed in the SI (Appendix D). As no significant amount of Fe was detected in the filtrate, it can be concluded that filtration at 0.2 µm efficiently removed goethite. The validity and the reproducibility of the results were confirmed using international geostandard SLRS-6.[43]

The metal ion adsorption onto goethite surface was expressed in percentage of metal ion adsorbed ($\%M_{ads}$) and the surface area-normalized distribution coefficient (K_d, L m^{-2}):

$$\%M_{ads} = \frac{[M]_{tot} - [M]_{aq}}{[M]_{tot}} \times 100 \quad (1)$$

$$K_d = \frac{[M]_{tot} - [M]_{aq}}{SSA \times \frac{m}{V} \times [M]_{aq}} \quad (2)$$

where $[M]_{tot}$ and $[M]_{aq}$ refer to the total (initial) metal ion concentration (in mol L^{-1}) and its concentration in solution after phase separation, respectively, *SSA* is the specific surface area of goethite expressed as m^2 kg^{-1} and *m/V* is the solid to liquid ratio expressed as mass of a solid in contact with a solution of a given volume (in kg L^{-1}). According to previous adsorption studies, ±5% was considered for the percentage adsorbed, ± 0.2 L m^{-2} for $\log_{10} K_d$ values was considered for REE except Sc, whose adsorption is moderate, and ± 0.5 L m^{-2} for Sc, Th and U whose adsorption is very strong.[44,45]

Surface complexation modeling (SCM). PHREEQC version 2 was used to model surface complexation onto goethite using thermodynamic database "Minteq v4".[46] Activity coefficients were calculated using Davies equation. Additionally, stability constants at 0 M ionic strength and 25 °C for REE (here except Sc) inorganic anion complexation were added in the database which includes (i) chloride ($REECl^{2+}$, $REECl_2^{+}$),[47] (ii) hydroxide ($REEOH^{2+}$, $REE(OH)_2^{+}$, $REE(OH)_3$),[48] (iii) bicarbonate and carbonate ($REEHCO_3^{2+}$, $REECO_3^{+}$ and $REE(CO_3)_2^{-}$),[49] as well as the solubility of freshly formed (amorphous) $REE(OH)_{3(am)}$ phases.[50] These references were chosen because they provide consistent data for the whole Ln and Y group, which is mandatory to model REE patterns, and because the original authors ensure internal consistency within this database. The details of the reactions and constants used are provided in a previous article[24] and summarized in supporting information (**Table S1,** Appendix E). Th and U database was taken from the Nuclear Energy Agency (NEA)[51,52] whereas Sc hydrolysis constants were

149 taken from the literature.[53] Model showed no precipitation of $REE(OH)_{3(am)}$, $Sc(OH)_{3(s)}$ or
150 Schoepite in the present experimental conditions.
151 Predictions of metal ion adsorption to goethite were made using Charge Distribution-Multi SIte
152 complexation (CD-MUSIC) model approach.[6–8,54] In this model, both singly ($\equiv FeOH^{-0.5}$) and
153 triply ($\equiv Fe_3O^{-0.5}$) coordinated oxygen were defined for reaction with the proton and background
154 electrolyte but only the singly coordinated groups were considered for metal adsorption. The
155 widely used '1pK approximation', allows to set the pK values (referring to the acidity constant)
156 of both singly and triply coordinated oxygens to the isoelectric point, which was assumed to
157 equal the point of zero charge (PZC). According to previous studies, synthetic goethite exhibits a
158 plane distribution of 27% (100) and 63% (110), and 10% (210) (group *Pbnm*).[6–8] Because planes
159 (100) and (110) show the same proportion of $\equiv FeOH^{-0.5}$ and $\equiv Fe_3O^{-0.5}$, they are generally not
160 distinguished in surface complexation models and a weighted average of their site densities is
161 used. The crystallographic site densities used were as follows:[7,8,54] 3.12 $\equiv FeOH^{-0.5}$ and $\equiv Fe_3O^{-0.5}$
162 nm^{-2} at the (110)/(100) planes (which represent together 90% of the surface) and 7.4 $\equiv FeOH^{-0.5}$
163 nm^{-2} at the (021) plane (which represents 10% of the surface). The interfacial electrostatics of the
164 system were defined by the Triple Layer Model (TLM)[55] where ions can be distributed between
165 the 0-, 1- and 2-planes (Δz_0; Δz_1; Δz_2). The electrostatics at the (110)/(100) and (021) faces were
166 independently treated. The solution-side part of the interface is described according to the Gouy-
167 Chapman equation.[56] The total (Stern) capacitance of the oxide/water interface is split into the
168 capacitances of the charge-free layers in between the 0-, 1- and 2-planes. For goethite, C_1 = 2.3
169 F/m^2 and C_2 = 1.07 F/m^2 (Cs = 0.73 F/m^2).[42] More details are provided in the SI of Marsac et al.
170 (2016)[54], and are repeated in the present SI for the sake of simplicity (Appendix E).

The charge of H^+ ions was placed at the surface (0-plane) whereas for Cl^- and Na^+ the charges were located at the 2-plane. The charge of REE, Th, and U ions was distributed at the goethite/water interface between 0-plane and 1-plane. As the presence of atmospheric $CO_{2(g)}$ dissolution was not avoided in our experiments, equilibrium with the atmosphere was considered in the calculations, because it might be reasonable to assume that, at $3 < pH < 7$, dissolved CO_2 concentration remains low and might equilibrate with the solution within less than 24h. Carbonate surface complexation to goethite was also considered, using reactions and parameters in **Table 1**,[57] although preliminary tests showed that binary carbonate-goethite complexes had insignificant effects on cations binding with goethite in the present conditions. By contrast, ternary U-carbonate-goethite complexes have been previously evidenced and modelled with CD-MUSIC (Table S2, Appendix E),[9,58,59] so they were considered in the present study. Charges of carbonate and U were distributed between the 0-plane and 1-plane. As further discussed later in this manuscript, our data do not evidence such complex for REE and Th, so no attempt to include them was made.

During the parameter fit, the charge variations at the 0-, 1-and 2-planes (Δz_0; Δz_1; Δz_2) were determined together with the surface complexation constants during the parameter estimation using PhreePlot,[60] which employs a modified Marquardt−Levenberg procedure.[61] Several constraints were applied in order to decrease the number of adjustable parameters. The charge variation was constrained equal at the (021) and (110)/(100) planes for all the metal ion reactions. In addition, cation charge (n) was distributed between planes 0 and 1, hence leading to the following relationships: $\Delta z_1 = n - \Delta z_0$ and $\Delta z_2 = 0$. Charge distribution for Ln and Y were set equal. Experimental REE $\log_{10} K_d$ patterns were used to constrain the pattern of the surface complexation constants[24] at the corresponding goethite faces. REE $\log_{10} K_d$ pattern at pH = 5.21

and $[M]_{tot} = 1\times10^{-7}$ M (denoted $K_{d,low}$) and $\log_{10} K_d$ pattern at pH = 6.42 and $[M]_{tot} = 7\times10^{-6}$ M (denoted $K_{d,high}$) were respectively selected for that purpose:

$$log_{10}\, K^{0}{}_{(021),\mathrm{Ln}} = a \times log_{10}\, K_{d,low} + b \quad (3)$$

$$log_{10}\, K^{0}{}_{(110)/(100),\mathrm{Ln}} = c \times log_{10}\, K_{d,high} + d \quad (4)$$

Where *a*, *b*, *c* and *d* are adjustable parameters of the linear relationships. Equations 3 and 4 were also applied to Y^{3+}.

Table 1. The CD-MUSIC model parameters for goethite protonation,[57,62,63] carbonate surface complexation[57] and surface electrostatics[a]. Charge variation at 0-, 1- and 2- planes is represented by Δz_0, Δz_1 and Δz_2, respectively.

Surface reaction	$\mathrm{Log_{10}\,K°}$	Δz_0	Δz_1	Δz_2
$\equiv Fe_3O^{-0.5} + H^+ \rightleftharpoons \equiv Fe_3OH^{+0.5}$	9.1	+1	0	0
$\equiv Fe_3O^{-0.5} + H^+ + Cl^- \rightleftharpoons \equiv Fe_3OHCl^{-0.5}$	8.1	+1	0	-1
$\equiv Fe_3O^{-0.5} + Na^+ \rightleftharpoons \equiv Fe_3ONa^{+0.5}$	-1	0	0	+1
$\equiv FeOH^{-0.5} + H^+ \rightleftharpoons \equiv FeOH_2{}^{+0.5}$	9.1	+1	0	0
$\equiv FeOH^{-0.5} + H^+ + Cl^- \rightleftharpoons \equiv FeOH_2Cl^{-0.5}$	8.1	+1	0	-1
$\equiv FeOH^{-0.5} + Na^+ \rightleftharpoons \equiv FeOHNa^{+0.5}$	-1	0	0	+1
$2(\equiv FeOH_2{}^{0.5+}) + CO_3{}^{2-} \rightleftharpoons \equiv (FeO)_2CO^- + 2H_2O$	-13.8	-1.33	-0.67	0
$2(\equiv FeOH_2{}^{0.5+}) + HCO_3{}^{-} \rightleftharpoons \equiv (FeO)_2COH + 2H_2O$	-18.7	-0.25	-0.75	0
$\equiv FeOH_2{}^{0.5+} + CO_3{}^{2-} \rightleftharpoons \equiv FeOCO_2{}^{1.5-} + H_2O$	-7.3	-1.35	-0.65	0
$\equiv FeOH_2{}^{0.5+} + HCO_3{}^{-} \rightleftharpoons \equiv FeOCOOH^{0.5-} + H_2O$	-7.9	-0.29	-0.71	0

[a]TPM with C_1 = 2.3 F m^{-2}, C_2 = 1.07 F m^{-2}. Site densities: $[\equiv FeOH^{-0.5}]$ = 3.12, and 7.4 site/nm^2 at the (110)/(100) and (021) planes, respectively; $[\equiv Fe_3O^{-0.5}]$ = 3.12 site/nm^2 at the (110)/(100) plane.

3. Results and discussion

Effects of pH and metal ion concentration on REE adsorption. The adsorption of Eu onto goethite versus pH in the presence of the other metal ions in 5 mM NaCl solution is shown in **Figure 2a** for $[M]_{tot}$ 1×10^{-7} M, 7×10^{-7} M and 7×10^{-6} M, referred to as low, intermediate and high metal concentrations, respectively. Data for all other Ln follow the same trend as Eu (**Figure S3, S4 and S5, Appendix F**). Ln binding to goethite surface increased with pH which is typical for cations adsorption onto metal oxides. However, sorption edge shifted to higher pH values when $[M]_{tot}$ was increased. This points to the saturation of a few number of strong sites occurring at the goethite surface, and predominant binding to weaker but more abundant sites at higher surface loadings. This is further supported by adsorption isotherm experiment (see **Figure 2b** and **S3**) in which adsorption drastically decreased in a first stage with increasing aqueous metal ion concentration due to saturation of adsorption sites. These results are in excellent agreement with previous studies,[6,9–11,64] where two different adsorption mechanisms onto goethite surface had been shown, as well as on hydrous ferric oxides,[2] hematite,[65] quartz,[24] and clays.[66] Accordingly, the high and low affinity sites for Ln and Y adsorption are hypothesized at two different crystallographic faces, (021) and (110)/(100) (**Figure 1**), as recently confirmed by X-ray-absorption spectroscopy.[12]

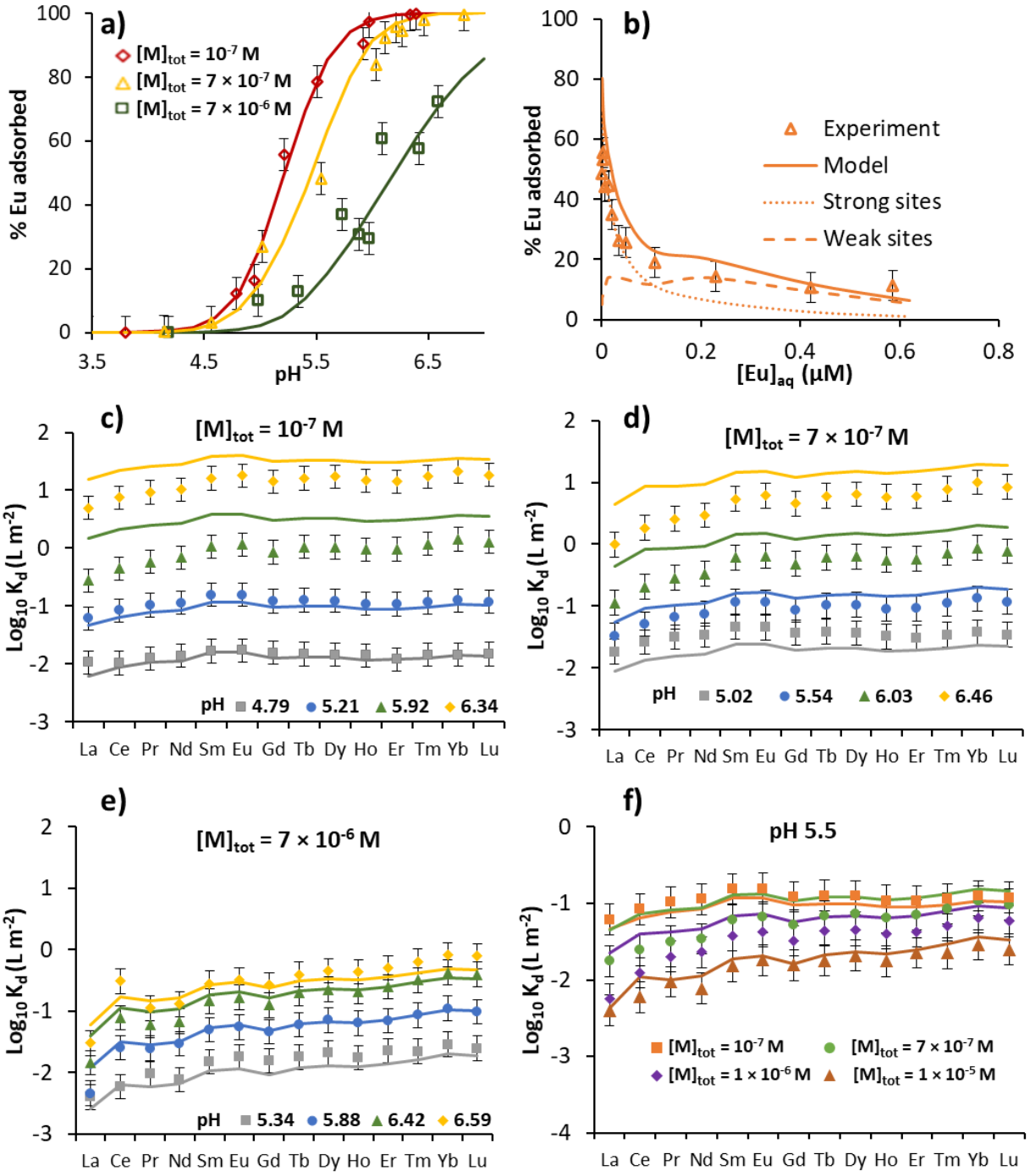

Figure 2. Percentage of Eu adsorbed as a function of (a) pH for different total metal ion concentrations ($[M]_{tot}$) and (b) final Eu aqueous concentration ($[Eu]_{aq}$) at pH 5.5. Corresponding REE Log_{10} K_d patterns at different pH values for total metal ion concentrations of (c) 1×10^{-7} M (d) 7×10^{-7} M (e) 7×10^{-6} M, and (f) at pH 5.5 for different metal ion concentrations. Experimental conditions: m/V = 0.1 g L^{-1}, temperature 20˚ C, reaction time 24 hours. All solid lines represent model. Error bars correspond to ±5% or ± 0.2 L m^{-2} for Log_{10} K_d.

REE patterns evolution. As Sc shows a distinct behavior from other REE, it was discussed separately. The REE K_d patterns obtained at different pH values corresponding to low, intermediate and high $[M]_{tot}$ (**Figure 2c, d & e**, respectively) show M-type tetrad effect which indicates inner-sphere complexation of REE at the goethite surface.[34,35] Additionally, two distinct patterns emerged at low $[M]_{tot}$ (**Figure 2c**) and high (**Figure 2e**) $[M]_{tot}$, with preferential adsorption of middle (MREE) and heavy (HREE) REE, respectively. This transition occurs from the former to the latter at intermediate $[M]_{tot}$ (**Figure 2d**) with increasing pH. The evolution of the REE pattern can be examined by comparing the Log_{10} K_d differences between two REE, such as Gd and Yb (denoted as Gd-Yb), especially when significant changes occur for HREE, as observed in this study. Values of Gd-Yb were plotted in **Figure 3a** versus the surface loading (in nm^{-2}), which was calculated based on the total concentrations of all adsorbed metal ions onto goethite:

$$Surface\ loading = \frac{\sum\left([M]_{tot} - [M]_{aq}\right) \times \mathrm{V} \times N_A \times 10^{-18}}{\mathrm{m} \times \mathrm{SSA}} \quad (5)$$

Where N_A is the Avogadro constant (mol^{-1}). Values of Gd-Yb progressively decreased with increasing loading until approximately 0.1 nm^{-2} where they reached kind of a plateau, albeit with scattering most probably arising from the lack of consideration of H^+ in equation 5. This observation suggests that saturation of strong binding sites on the (021) plane occurred at surface loadings below 0.1 nm^{-2}. This finding supports the hypothesis of two distinct surface complexation mechanisms governing REE binding with goethite at low and high surface loadings, potentially due to differing coordination environments at the (021) and (110)/(100) faces. Theoretically, as the (021) face represents 10% of the surface area, the site density of $\equiv FeOH^{-0.5}_{(021)}$ approximately equals 0.74 nm^{-2} when normalized to the whole surface.[7,8] This

leads to a theoretical bidentate edge sharing complex (i.e. strong site) density of 0.37 m^{-2}. The observed surface loading at which site saturation occurs is lower than this value, likely due to electrostatic repulsions generated by cation adsorption at high surface loadings.

Y-Ho fractionation. The pH-edge envelope of Y (**Figures S4** & **S5**) exhibited a concentration dependence similar to Ln, consistent with its analogous geochemical behavior to Ho (one of the Ln) due to similar charge and ionic radii.[67] However, at any given pH and $[M]_{tot}$ the percentage of Y adsorbed is consistently lower than that of Ho, indicating Y-Ho fractionation. This phenomenon, previously observed on calcite, Fe- and Mn-oxide surfaces,[35,68,69] is attributed to the more covalent nature of Ho-O bonding at the goethite surface due to 4f orbital participation compared to Y-O bonding.[67,69] The degree of Y-Ho fractionation, quantified by the differences in their respective Log_{10} K_d values, increases with pH,[36,38] (**Figure S6a**) and depends on surface loading (**Figure 3b**), which in turn is influenced by pH. Y-Ho fractionation tends to be steady at surface loadings above approximately 0.1 nm^{-2}, similar to the pattern observed for Ln (**Figure 3a**). This observation supports the notion of a change in surface speciation for Y, favoring the formation of more covalent bonds with the $\equiv FeOH^{-0.5}$ sites of the (110)/(100) face.

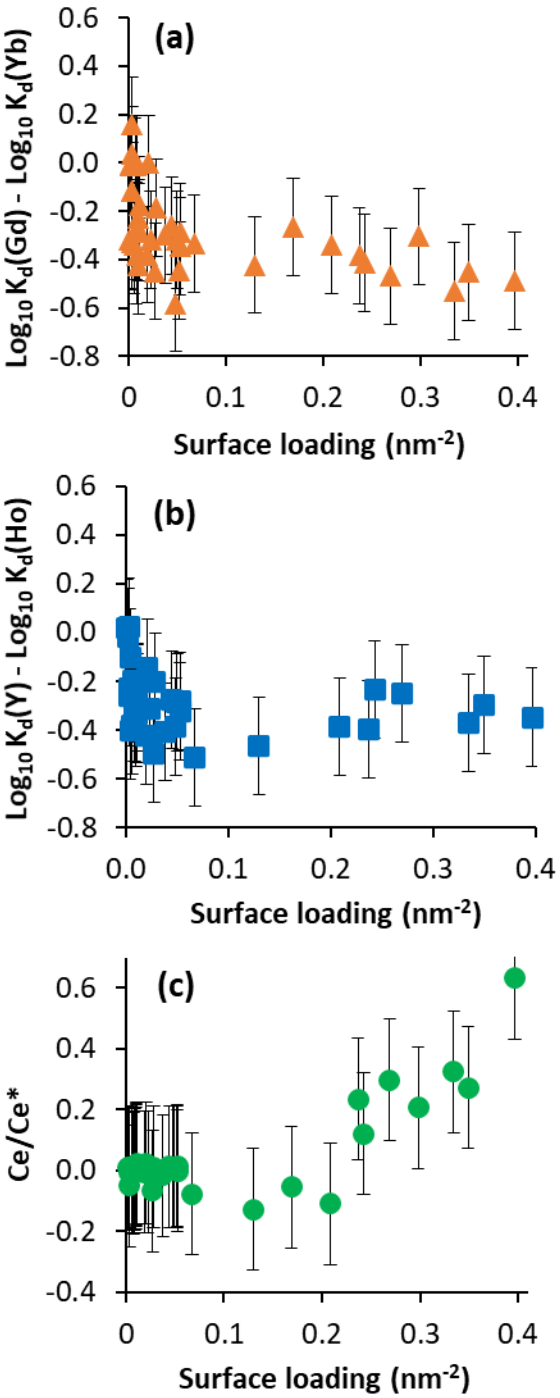

Figure 3. Difference in $\log_{10} K_d$ values of (a) Gd and Yb, and (b) Y and Ho plotted *vs.* surface loading (eq. (5) (c) Ce anomaly (Ce/Ce*; eq. (6) *vs.* surface loading. Error bars correspond to ± 0.2 L m^{-2} of $\text{Log}_{10} K_d$.

Anomalous behavior of Ce. Positive Ce anomaly (Ce/Ce*) was observed on REE patterns (**Figures 2e, f**), due to the oxidation of Ce(III) to Ce(IV) at the goethite surface.[36,38,70] This anomaly can be quantified using the following relationship:

$$Ce/Ce* = \mathrm{Log}_{10}\left(\frac{\mathrm{K}_d^{Ce}}{\frac{1}{2}(\mathrm{K}_d^{La} + \mathrm{K}_d^{Pr})}\right) \quad (6)$$

Ce-anomaly serves as a useful indicator of prevailing redox conditions or the redox capacity of the adsorbing phase. While Fe(III) ions in goethite are not strong enough to oxidize Ce(III) to Ce(IV),[71] recent work by Ratié et al.,[70] suggests that Ce oxidation can be driven by O_2 through the formation of a more thermodynamically favorable Ce(IV)-oxide or -hydroxide ($CeO_{2(s)}$ or $Ce(OH)_{4(s)}$) at high $[Ce]_{tot}$ (e.g. in the order of 10^{-5} M or above), as shown below (for the case of $Ce(OH)_{4(s)}$):

$$Ce^{3+} + 4H_2O \rightleftharpoons Ce(OH)_{4(s)} + 4H^+ + e^- \quad (7)$$

The larger Ce-anomaly at the highest $[M]_{tot}$ investigated seem to corroborate this conclusion (see **Figure S6b**). Although the formation of Ce(IV)-containing nanoparticles could not be observed by TEM in a similar study focusing only on Ce, even at larger Ce concentrations than presently investigated,[70] the formation of nanoparticle or surface precipitates remains plausible as it was observed on goethite for other tetravalent actinides analogous of Ce(IV) (e.g. $PuO_{2(s)}$).[72] However, the precipitation of Ce(IV)-(hydr)oxide may not fully explain Ce redox speciation at low $[Ce]_{tot}$ ($4\times10^{-9} < [Ce]_{tot} < 4\times10^{-7}$ M). In **Figure 3c**, plotting Ce/Ce* versus the surface loading revealed that the anomaly developed at loadings above approximately 0.2 nm^{-2}, which is of the same order of magnitude as the $\equiv FeOH^{-0.5}$ sites on the (021) face. By analogy with Pu,

where Pu(IV) adsorption to minerals was significantly stronger than Pu(III),[73–76] we suggest that larger Ce-anomaly arises from higher relative affinity of Ce(IV) over Ce(III) at high loadings compared to low loadings and, hence, might be related to the shift in REE surface speciation from the (021) to the (110)/(100) faces of goethite. This will be discussed further by inspecting Th(IV) behavior, here used as an analogue of Ce(IV),[40] in the next section.

Th(IV) as analogue of Ce(IV). Thorium occurs as a tetravalent cation resulting in its strong surface complexation with goethite (**Figure 4a**). As the final aqueous concentration of Th measured was below its solubility limit with respect to amorphous $Th(OH)_{4(s)}$ formation (**Figure S7, Appendix G**), it is suggested that Th removal from the solution is mainly driven by surface complexation rather than precipitation. The significantly enhanced adsorption of Th(IV), in comparison to trivalent Ln, across a wide range of pH values and metal concentrations (**Figures 2, S4** & **S5**), falls in line with greater stabilization of Ce(IV) over Ce(III) at the goethite surface. Thorium adsorption exhibits almost no dependence on pH (K_d on the order of 10^3 L m^{-2}), as commonly observed for tetravalent actinides (Th, Np or Pu) at clay minerals, silica or iron oxides at pH > 3.[73,75,77] Additionally, K_d(Th) remains nearly independent of $[M]_{tot}$, under the present experimental conditions. This points to the predominant surface complexation of Th(IV) at the (021) sites under all conditions, as confirmed by (i) its ability to potentially outcompete with all the other investigated metal ions, and (ii) its surface loading never exceeding 0.032 nm^{-2}, below the strong site density. As increasing $[M]_{tot}$ decreases K_d(REE), the corresponding increase in the K_d(Th)/K_d(REE) ratio indicates higher relative affinity of tetravalent over trivalent metal ions for goethite surface at high loadings. This further supports the hypothesis that Ce-anomaly is more pronounced at high loadings because of the facet-dependent metal ions adsorption onto goethite. This proposed mechanism for Ce-anomaly development offers the advantage of applicability

across any $[Ce]_{tot}$ conditions, unlike $Ce(OH)_{4(am)}$ which is restricted to supersaturated systems. Additionally, it may explain Ce redox speciation variations observed on distinct mineral phases under ambient atmosphere where similar redox conditions are presumed to prevail.[70]

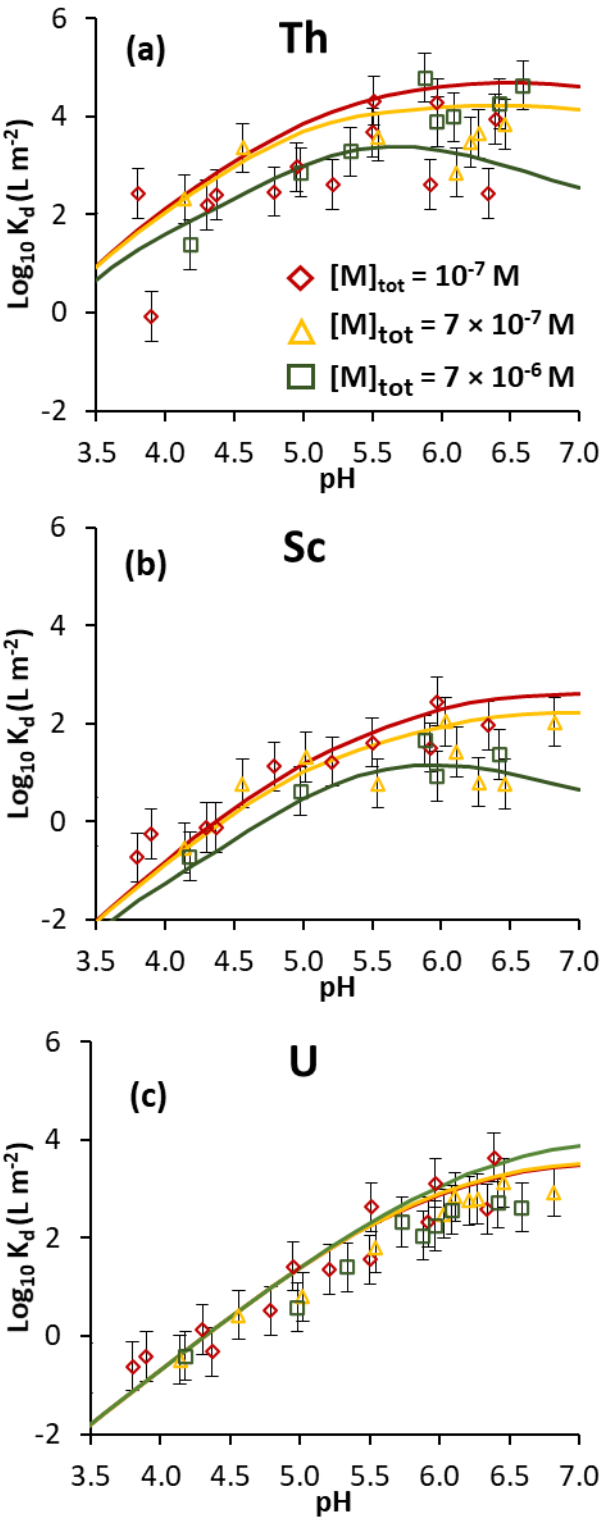

320

321 **Figure 4**. Adsorption expressed as $\log_{10} K_d$ (L m^{-2}) as a function of pH for different total metal
322 ion concentrations ($[M]_{tot}$) for (a) Th (b) Sc and (c) U. Error bars correspond to ± 0.5 L m^{-2} of
323 $\text{Log}_{10} K_d$.
324

Sc(III) and U(VI). As Sc shows a distinct behavior from other REE, it was discussed separately and the comparative adsorption of REE was extended to encompass U, as they might co-occur and compete with REE for goethite surface sites, and provide complementary information to probe goethite surface reactivity. Scandium showed stronger adsorption compared to Ln and Y (**Figures S4** & **S5**), which can be explained by the smaller ionic radius of Sc^{3+} as compared to Lu^{3+} (0.87 *vs*. 0.98 Å, for CN = 8).[67] In fact, its adsorption behavior lies intermediary between that of REE, because it is pH-dependent, and Th, which remains largely unaffected by variations in $[M]_{tot}$ (**Figures S4** & **S5**). This suggests that Sc preferentially binds to the (021) face in any investigated conditions, like Th. In a previous study,[78] Sc was shown to form mainly bidentate corner sharing complexes at the (110)/(100) surface of goethite using X-ray absorption spectroscopy (XAS) analyses. However, these experiments were conducted with significantly higher $[Sc]_{tot}$ (2.22×10^{-4} M) as compared to the present $[M]_{tot}$ (7×10^{-6} M), under similar conditions (i.e. ionic strength, m/V and pH range, etc). This may lead to insignificant contribution of the spectroscopic signal of Sc bound to the (021) face. Uranium (U), under oxic conditions, is expected to occur as uranyl ion (UO_2^{2+}) in aqueous solutions, behaving as a cation with an effective charge of +3.3.[79] This explains its stronger adsorption to goethite than that of REE. However, in contrast to the other investigated metal ions, the adsorption of U(VI) onto goethite also involved U-carbonate ternary complexes (**Table S2**).[9,57] The present results for U are also in agreement with previous studies of U complexation with Fe oxides.[9,80–82]

Surface complexation modeling. The surface complexation reactions of all Ln^{3+} except Pm, as well as Sc^{3+}, Y^{3+}, and UO_2^{2+} ions (denoted by M^{n+}), could be expressed by the following reaction, as suggested by previous spectroscopic studies:[9,12,78]

$$2(\equiv FeOH^{-0.5}) + M^{n+} \rightleftharpoons (\equiv FeOH^{-0.5})_2 M^{+(n-1)} \quad (8)$$

Equation 8 does not explicitly specify the number of involved Fe(III) octahedra in the reaction, as it solely indicates the number of $\equiv FeOH^{-0.5}$ sites that may or may not be associated with the same Fe(III) octahedron. Therefore, equation 8 can be applied to both the bidentate edge- and corner-sharing surface complexation processes at the (021) and (110)/(100) faces of goethite, respectively.[10,78] Although spectroscopic investigations have not been performed to confirm the formation of both complexes, for the sake of consistency, the same surface complexation reactions were considered for all metal ions at both faces.

As no redox potential (E_H) measurements could be made in this study under ambient atmosphere, no redox speciation of Ce could be modeled using PHREEQC and CD-MUSIC. Indeed, the E_H and surface complexation constants for Ce(III) and Ce(IV) should be treated as adjustable parameters in the model, which would lead to an infinite number of mathematical solutions as the E_H and [Ce(IV)]/[Ce(III]) are related via the Nernst equation. Instead, only Ce(III) is considered in the calculation (by artificially setting an extremely low value for the standard redox potential of the Ce(IV)/Ce(III) couple) and two $\log_{10} K^0$ values for Ce at the (021) are proposed. It allows a semi-quantitative prediction of (i) Ce(III) binding to goethite, by taking the mean $\log_{10} K^0$ values between La and Pr, to account for the expected absence of Ce-anomaly in moderately reducing conditions (where Ce(IV) is negligible), and (ii) Ce-anomaly under oxic conditions (similar to the present ones), by fitting the Ce experimental data, as previously done.[26]

Concerning U, reactions and parameters for UO_2^{2+} were taken from the literature,[57] except for the charge variation and formation constant of $(\equiv FeOH)_2UO_2CO_3^-$ that were optimized in phreeplot in order to accommodate the differences in electrostatics and description of the goethite surface between previous work and the present study (See **Table S2 & S3)**. Preliminary tests revealed that Th adsorption was underestimated at high pH and loadings (pH > 6.2). Therefore, Th adsorption was assumed to involve the second hydrolysis expressed as:

$$2(\equiv FeOH^{-0.5}) + Th^{4+} + 2H_2O \rightleftharpoons (\equiv FeOH^{-0.5})_2Th(OH)_2^+ + 2H^+ \quad (9)$$

All model parameters are presented in **Table 2**, using constraints described in the materials and methods section. Results of the fit performed using Phreeplot (presented in **Figures 2, 3 & 4**), show that the model can predict the effects of pH and surface loading on the adsorption on each studied metal ion. REE surface speciation simulations captured relatively well the transition from strong sites, dominant at low loadings, i.e. at low $[M]_{tot}$ (**Figure S8a, Appendix H**) or at intermediate one but at pH < 6 (**Figure S8b**), to weak sites dominant at higher loadings, i.e. at high $[M]_{tot}$ (**Figure S8c**) or at intermediate one for pH > 6 (**Figure S8b**). The surface complexation model captured well the corresponding change in the Ln pattern (**Figures 2c-e**), as well as Ce-anomaly development (**Figures 2c-f**). As previously anticipated for Th and Sc adsorption, the model shows predominant binding to the (021) face and the absence of amorphous $Th(OH)_{4(s)}$ precipitation, which explains the small dependence to $[M]_{tot}$ simulated (**Figures 4a, b**). The smaller changes in the surface speciation for Th(IV) for most of the investigated pH range (**Figure S9**), in contrast to the widely evolving speciation of REE(III) in response to varying surface loading, further consolidates the hypothesis of the facet-dependent

development of Ce-anomaly. In agreement, with previous studies, U surface complexation to goethite was well predicted by accounting for the formation of ternary goethite-U-carbonate complexes (**Figure 4c**). The multi-element REE surface complexation model developed in this study demonstrated its capability to predict the sorption behavior of mono-element REE (La, Eu or Nd) in the literature (See **Table S3** & **Figure S10, Appendix I**).[64,83–85] This shows that the developed surface complexation model can be effectively applied to other systems under different geochemical conditions, including varying metal concentrations and different goethite morphology and surface.

Table 2. Surface complexation model parameters for all Ln except Pm, as well as Sc, Y and Th sorption onto goethite. Charge variation at (021) and (110)/(100) faces were set equal for each ion. Parameters of equations (8) and (9) were: a = 0.96 ± 0.09, b = 12.38 ± 0.06, c = 0.81 ± 0.08, d = 11.06 ± 0.34. [(1)]Obtained by fitting of Ce data. [(2)]Average value between La and Pr.

Surface species	Log_{10} $K°_{(110)/(100)}$	Log_{10} $K°_{(021)}$	Δz_0; Δz_1; Δz_2
$\equiv (FeOH^{-0.5})_2La^{2+}$	13.55± 0.55	15.92± 0.25	0.65; 2.35; 0
$\equiv (FeOH^{-0.5})_2Ce^{2+}$	14.14± 0.56[(1)] 13.80± 0.55[(2)]	16.05± 0.25[(1)] 16.03± 0.25[(2)]	
$\equiv (FeOH^{-0.5})_2Pr^{2+}$	14.04± 0.57	16.14± 0.26	
$\equiv (FeOH^{-0.5})_2Nd^{2+}$	14.09± 0.57	16.17± 0.26	
$\equiv (FeOH^{-0.5})_2Sm^{2+}$	14.36± 0.59	16.31± 0.26	
$\equiv (FeOH^{-0.5})_2Eu^{2+}$	14.41± 0.60	16.31± 0.26	
$\equiv (FeOH^{-0.5})_2Gd^{2+}$	14.31± 0.59	16.21± 0.26	
$\equiv (FeOH^{-0.5})_2Tb^{2+}$	14.46± 0.60	16.22± 0.25	
$\equiv (FeOH^{-0.5})_2Dy^{2+}$	14.51± 0.60	16.21± 0.25	
$\equiv (FeOH^{-0.5})_2Ho^{2+}$	14.49± 0.60	16.16± 0.25	
$\equiv (FeOH^{-0.5})_2Er^{2+}$	14.55± 0.60	16.16± 0.25	
$\equiv (FeOH^{-0.5})_2Tm^{2+}$	14.64± 0.61	16.18± 0.25	
$\equiv (FeOH^{-0.5})_2Yb^{2+}$	14.74± 0.61	16.22± 0.25	
$\equiv (FeOH^{-0.5})_2Lu^{2+}$	14.71± 0.61	16.20± 0.25	
$\equiv (FeOH^{-0.5})_2Y^{2+}$	14.19 ± 0.57	15.97± 0.25	
$\equiv (FeOH^{-0.5})_2Sc^{2+}$	18.94 ± 0.9	20.33 ± 0.5	1.96; 1.04; 0
$\equiv (FeOH^{-0.5})_2Th(OH)_2^+$	8.22 ± 1.73	12.02 ± 0.37	0.89; 1.11; 0

4. Environmental implications

Adsorption onto Fe-oxyhydroxides is controlled by their distinct crystal facets, with varying surface properties and binding sites. Using REE as surface probe and variations in REE patterns, we notably demonstrated the influence of facet-dependent adsorption of goethite on REE sorption and Ce redox speciation. Specifically, we observed a preference for middle REE (MREE) and heavy REE (HREE) adsorption on the (021) and (110)/(100) faces of goethite, respectively. This may have major impact in utilization of REE pattern variations in different geochemical systems, where goethite occurs. Ce-anomaly was observed at higher metal loadings, associated with shifts in REE(III) surface speciation from (021) to (110)/(100) faces of goethite. Enhanced stabilization of Ce(IV) as compared to Ce(III) on the goethite surface because of the predominant adsorption of Ce(IV) onto the (021) face and high relative Ce(IV)/Ce(III) affinity at high loadings was also observed. This newly proposed mechanism to explain the development of Ce-anomaly holds applicability across a range of $[Ce]_{tot}$ conditions and offers insights into Ce redox speciation across diverse mineral phases under ambient atmospheric conditions. This has substantial implications for the mobility of Ce, as well as other redox-sensitive elements, in natural systems where similar redox conditions may prevail. This study holds significant relevance for understanding paleoredox environments, particularly in relation to the use of Ce anomalies as a geochemical indicator. The surface complexation model developed in this study not only enables the prediction of REE behavior in complex competitive systems with Sc, Th and U, but also provides insights into Y-Ho fractionation and Ce oxidation on the goethite surface under ambient atmospheric conditions. Given that REE are emerging contaminants, this study provides a powerful predictive tool to help in understanding molecular-level processes governing REE fate and transport within complex environmental mixtures.

5. Supporting Information

(A) Additional details for materials and methods; (B) synthesis and characterization of goethite; (C) batch kinetic experiments between goethite and REE, U and Th; (D) metal ions concentration determination by ICP-MS; (E) modeling: goethite morphology and site density calculation, database used for REE(III), Sc and Y, surface complexation reactions for U; (F) experimental adsorption results; (G) Th solubility; (H) Surface speciation for Eu and Th; (I) Prediction of existing literature data.

6. Acknowledgments

This project has received funding from the European Union's Horizon 2020 research and innovation program under the Marie Sklodowska-Curie Grant Agreement No. 857989 (PANORAMA project) and the COLOSSAL project funded by ANR (project number ANR-23-CE01-0001). The authors are grateful for the support of the GeOHeLiS analytical platform of Rennes. Through this platform, this publication is also supported by the European Union through the European Regional Development Fund (FEDER), the French ministry of Higher Education and Research, the French Region of Brittany and Rennes Métropole.

7. References

(1) Cornell, R. M.; Schwertmann, U. *The Iron Oxides: Structure, Properties, Reactions, Occurrences, and Uses*; Wiley-vch Weinheim, 2003; Vol. 664.
(2) Dzombak, D. A.; Morel, F. M. *Surface Complexation Modeling: Hydrous Ferric Oxide*; John Wiley & Sons, 1990.
(3) Jickells, T. D.; An, Z. S.; Andersen, K. K.; Baker, A. R.; Bergametti, G.; Brooks, N.; Cao, J. J.; Boyd, P. W.; Duce, R. A.; Hunter, K. A.; Kawahata, H.; Kubilay, N.; laRoche, J.; Liss, P. S.; Mahowald, N.; Prospero, J. M.; Ridgwell, A. J.; Tegen, I.; Torres, R. Global Iron Connections Between Desert Dust, Ocean Biogeochemistry, and Climate. *Science* **2005**, *308* (5718), 67–71. https://doi.org/10.1126/science.1105959.
(4) Schwertmann, U.; Cornell, R. M. *Iron Oxides in the Laboratory: Preparation and Characterization*; John Wiley & Sons, 2008.
(5) Hiemstra, T.; De Wit, J. C. M.; Van Riemsdijk, W. H. Multisite Proton Adsorption Modeling at the Solid/Solution Interface of (Hydr)Oxides: A New Approach: II. Application to Various Important (Hydr)Oxides. *Journal of Colloid and Interface Science* **1989**, *133* (1), 105–117. https://doi.org/10.1016/0021-9797(89)90285-3.
(6) Hiemstra, T.; Van Riemsdijk, W. H. A Surface Structural Approach to Ion Adsorption: The Charge Distribution (CD) Model. *Journal of Colloid and Interface Science* **1996**, *179* (2), 488–508. https://doi.org/10.1006/jcis.1996.0242.
(7) Boily, J.-F.; Lützenkirchen, J.; Balmès, O.; Beattie, J.; Sjöberg, S. Modeling Proton Binding at the Goethite (α-FeOOH)-Water Interface. *Colloids and Surfaces A: Physicochemical and Engineering Aspects* **2001**, *179* (1), 11–27. https://doi.org/10.1016/S0927-7757(00)00712-3.
(8) Gaboriaud, F.; Ehrhardt, J.-J. Effects of Different Crystal Faces on the Surface Charge of Colloidal Goethite (α-FeOOH) Particles: An Experimental and Modeling Study.

Geochimica et Cosmochimica Acta **2003**, *67* (5), 967–983. https://doi.org/10.1016/S0016-7037(02)00988-2.
(9) Sherman, D. M.; Peacock, C. L.; Hubbard, C. G. Surface Complexation of U (VI) on Goethite (α-FeOOH). *Geochimica et Cosmochimica Acta* **2008**, *72* (2), 298–310.
(10) Ugwu, I. M.; Sherman, D. M.; Bacon, C. G. D. Sorption of Nickel Ontogoethite (α-FeOOH) and Desorption Kinetics of Aged Synthetic Ni-Goethite: Implication for Ni Laterite Ore. *Chemical Geology* **2019**, *509*, 223–233. https://doi.org/10.1016/j.chemgeo.2019.01.013.
(11) Wu, J.; Zhao, X.; Li, Z.; Gu, X. Thermodynamic and Kinetic Coupling Model of Cd(II) and Pb(II) Adsorption and Desorption on Goethite. *Science of The Total Environment* **2020**, *727*, 138730. https://doi.org/10.1016/j.scitotenv.2020.138730.
(12) Buist, A.; Rivard, C.; Davranche, M.; Brisset, F.; Hanna, K.; Paineau, E.; Rouzière, S.; Elkaim, E.; Blanchandin, S.; Chaouchi, K.; Hotton, C.; Dia, A.; Vantelon, D. Impact of Aluminium and Gallium Substitutions on the Ferrihydrite and Goethite Structure: Consequences for Rare Earth Element Adsorption and Complexation. *Chemical Geology* **2024**, *667*, 122312. https://doi.org/10.1016/j.chemgeo.2024.122312.
(13) Venema, P.; Hiemstra, T.; Van Riemsdijk, W. H. Multisite Adsorption of Cadmium on Goethite. *Journal of Colloid and Interface Science* **1996**, *183* (2), 515–527. https://doi.org/10.1006/jcis.1996.0575.
(14) Livi, K. J. T.; Villalobos, M.; Leary, R.; Varela, M.; Barnard, J.; Villacís-García, M.; Zanella, R.; Goodridge, A.; Midgley, P. Crystal Face Distributions and Surface Site Densities of Two Synthetic Goethites: Implications for Adsorption Capacities as a Function of Particle Size. *Langmuir* **2017**, *33* (36), 8924–8932. https://doi.org/10.1021/acs.langmuir.7b01814.
(15) Livi, K. J. T.; Villalobos, M.; Ramasse, Q.; Brydson, R.; Salazar-Rivera, H. S. Surface Site Density of Synthetic Goethites and Its Relationship to Atomic Surface Roughness and Crystal Size. *Langmuir* **2023**, *39* (1), 556–562. https://doi.org/10.1021/acs.langmuir.2c02818.
(16) Zhou, B.; Li, Z.; Chen, C. Global Potential of Rare Earth Resources and Rare Earth Demand from Clean Technologies. *Minerals* **2017**, *7* (11), 203. https://doi.org/10.3390/min7110203.
(17) Drobniak, A.; Mastalerz, M. Rare Earth Elements: A Brief Overview. *Indiana Journal of Earth Sciences* **2022**, *4*. https://doi.org/10.14434/ijes.v4i1.33628.
(18) Kulaksız, S.; Bau, M. Anthropogenic Dissolved and Colloid/Nanoparticle-Bound Samarium, Lanthanum and Gadolinium in the Rhine River and the Impending Destruction of the Natural Rare Earth Element Distribution in Rivers. *Earth and Planetary Science Letters* **2013**, *362*, 43–50. https://doi.org/10.1016/j.epsl.2012.11.033.
(19) Langkau, S.; Erdmann, M. Environmental Impacts of the Future Supply of Rare Earths for Magnet Applications. *Journal of Industrial Ecology* **2020**, jiec.13090. https://doi.org/10.1111/jiec.13090.
(20) Egler, S. G.; Roldão, T. M.; Santos, G. O.; Heidelmann, G. P.; Giese, E. C.; Correia, F. V.; Saggioro, E. M. Acute Toxicity of Single and Combined Rare Earth Element Exposures towards Daphnia Similis. *Ecotoxicology and Environmental Safety* **2023**, *251*, 114538. https://doi.org/10.1016/j.ecoenv.2023.114538.

(21) German, C. R.; Elderfield, H. Application of the Ce Anomaly as a Paleoredox Indicator: The Ground Rules. *Paleoceanography* **1990**, *5* (5), 823–833. https://doi.org/10.1029/PA005i005p00823.
(22) Johannesson, K. H.; Stetzenbach, K. J.; Hodge, V. F. Rare Earth Elements as Geochemical Tracers of Regional Groundwater Mixing. *Geochimica et Cosmochimica Acta* **1997**, *61* (17), 3605–3618.
(23) Dia, A.; Gruau, G.; Olivié-Lauquet, G.; Riou, C.; Molénat, J.; Curmi, P. The Distribution of Rare Earth Elements in Groundwaters: Assessing the Role of Source-Rock Composition, Redox Changes and Colloidal Particles. *Geochimica et Cosmochimica Acta* **2000**, *64* (24), 4131–4151. https://doi.org/10.1016/S0016-7037(00)00494-4.
(24) Iqbal, M.; Marsac, R.; Davranche, M.; Dia, A.; Hanna, K. A Mechanistic Surface Complexation Approach for the Prediction of Rare Earth Element Reactive Transport in Quartz Porous Media. *Chemical Geology* **2023**, *634*, 121601. https://doi.org/10.1016/j.chemgeo.2023.121601.
(25) Quinn, K. A.; Byrne, R. H.; Schijf, J. Comparative Scavenging of Yttrium and the Rare Earth Elements in Seawater: Competitive Influences of Solution and Surface Chemistry. *Aquatic Geochemistry* **2004**, *10* (1–2), 59–80. https://doi.org/10.1023/B:AQUA.0000038959.03886.60.
(26) Pourret, O.; Davranche, M. Rare Earth Element Sorption onto Hydrous Manganese Oxide: A Modeling Study. *Journal of Colloid and Interface Science* **2013**, *395*, 18–23. https://doi.org/10.1016/j.jcis.2012.11.054.
(27) Coppin, F.; Berger, G.; Bauer, A.; Castet, S.; Loubet, M. Sorption of Lanthanides on Smectite and Kaolinite. *Chemical Geology* **2002**, *182* (1), 57–68. https://doi.org/10.1016/S0009-2541(01)00283-2.
(28) Takahashi, Y.; Châtellier, X.; Hattori, K. H.; Kato, K.; Fortin, D. Adsorption of Rare Earth Elements onto Bacterial Cell Walls and Its Implication for REE Sorption onto Natural Microbial Mats. *Chemical Geology* **2005**, *219* (1), 53–67. https://doi.org/10.1016/j.chemgeo.2005.02.009.
(29) Takahashi, Y.; Yamamoto, M.; Yamamoto, Y.; Tanaka, K. EXAFS Study on the Cause of Enrichment of Heavy REEs on Bacterial Cell Surfaces. *Geochimica et Cosmochimica Acta* **2010**, *74* (19), 5443–5462. https://doi.org/10.1016/j.gca.2010.07.001.
(30) Zoll, A. M.; Schijf, J. A Surface Complexation Model of YREE Sorption on Ulva Lactuca in 0.05-5.0M NaCl Solutions. *Geochimica et Cosmochimica Acta* **2012**, *97*, 183–199. https://doi.org/10.1016/j.gca.2012.08.022.
(31) Blancho, F.; Davranche, M.; Marsac, R.; Léon, A.; Dia, A.; Grassl, B.; Reynaud, S.; Gigault, J. Metal-Binding Processes on Nanoplastics: Rare Earth Elements as Probes. *Environmental Science: Nano* **2022**, *9* (6), 2094–2103. https://doi.org/10.1039/D2EN00048B.
(32) Catrouillet, C.; Guenet, H.; Pierson-Wickmann, A.-C.; Dia, A.; LeCoz, M. B.; Deville, S.; Lenne, Q.; Suko, Y.; Davranche, M. Rare Earth Elements as Tracers of Active Colloidal Organic Matter Composition. *Environ. Chem.* **2019**, *17* (2), 133–139. https://doi.org/10.1071/EN19159.
(33) Marsac, R.; Catrouillet, C.; Davranche, M.; Bouhnik-Le Coz, M.; Briant, N.; Janot, N.; Otero-Fariña, A.; Groenenberg, J. E.; Pédrot, M.; Dia, A. Modeling Rare Earth Elements Binding to Humic Acids with Model VII. *Chemical Geology* **2021**, *567*, 120099. https://doi.org/10.1016/j.chemgeo.2021.120099.

(34) Takahashi, Y.; Tada, A.; Kimura, T.; Shimizu, H. Formation of Outer- and Inner-Sphere Complexes of Lanthanide Elements at Montmorillonite-Water Interface. *Chemistry Letters - CHEM LETT* **2000**, *29*, 700–701. https://doi.org/10.1246/cl.2000.700.
(35) Ohta, A.; Kagi, H.; Nomura, M.; Tsuno, H.; Kawabe, I. Coordination Study of Rare Earth Elements on Fe Oxyhydroxide and Mn Dioxides: Part II. Correspondence of Structural Change to Irregular Variations of Partitioning Coefficients and Tetrad Effect Variations Appearing in Interatomic Distances. *American Mineralogist* **2009**, *94* (4), 476–486. https://doi.org/10.2138/am.2009.2987.
(36) Ohta, A.; Kawabe, I. REE(III) Adsorption onto Mn Dioxide (δ-MnO2) and Fe Oxyhydroxide: Ce(III) Oxidation by δ-MnO2. *Geochimica et Cosmochimica Acta* **2001**, *65* (5), 695–703. https://doi.org/10.1016/S0016-7037(00)00578-0.
(37) Davranche, M.; Pourret, O.; Gruau, G.; Dia, A.; Le Coz-Bouhnik, M. Adsorption of REE(III)-Humate Complexes onto MnO2: Experimental Evidence for Cerium Anomaly and Lanthanide Tetrad Effect Suppression. *Geochimica et Cosmochimica Acta* **2005**, *69* (20), 4825–4835. https://doi.org/10.1016/j.gca.2005.06.005.
(38) Bau, M. Scavenging of Dissolved Yttrium and Rare Earths by Precipitating Iron Oxyhydroxide: Experimental Evidence for Ce Oxidation, Y-Ho Fractionation, and Lanthanide Tetrad Effect. *Geochimica et Cosmochimica Acta* **1999**, *63* (1), 67–77. https://doi.org/10.1016/S0016-7037(99)00014-9.
(39) Kursun, I.; Terzi, M.; Tombal, T. D. HCl Leaching Behaviour of a Bastnasite Ore in Terms of Thorium and Rare Earth Elements. *Russ. J. Non-Ferrous Metals* **2016**, *57* (3), 187–194. https://doi.org/10.3103/S106782121603010X.
(40) Marsac, R.; Réal, F.; Banik, N. L.; Pédrot, M.; Pourret, O.; Vallet, V. Aqueous Chemistry of Ce(IV): Estimations Using Actinide Analogues. *Dalton Trans.* **2017**, *46* (39), 13553–13561. https://doi.org/10.1039/C7DT02251D.
(41) Cheng, W.; Li, J.; Sun, J.; Luo, T.; Marsac, R.; Boily, J.-F.; Hanna, K. Nalidixic Acid and Fe(II)/Cu(II) Coadsorption at Goethite and Akaganéite Surfaces. *Environ. Sci. Technol.* **2023**, *57* (41), 15680–15692. https://doi.org/10.1021/acs.est.3c05727.
(42) Hanna, K.; Martin, S.; Quilès, F.; Boily, J.-F. Sorption of Phthalic Acid at Goethite Surfaces under Flow-Through Conditions. *Langmuir* **2014**, *30* (23), 6800–6807. https://doi.org/10.1021/la4049715.
(43) Yeghicheyan, D.; Aubert, D.; Bouhnik- Le Coz, M.; Chmeleff, J.; Delpoux, S.; Djouraev, I.; Granier, G.; Lacan, F.; Piro, J.; Rousseau, T.; Cloquet, C.; Marquet, A.; Menniti, C.; Pradoux, C.; Freydier, R.; Vieira da Silva- Filho, E.; Suchorski, K. A New Interlaboratory Characterisation of Silicon, Rare Earth Elements and Twenty- Two Other Trace Element Concentrations in the Natural River Water Certified Reference Material SLRS - 6 (NRC - CNRC). *Geostand Geoanal Res* **2019**, *43* (3), 475–496. https://doi.org/10.1111/ggr.12268.
(44) Schnurr, A.; Marsac, R.; Rabung, T.; Lützenkirchen, J.; Geckeis, H. Sorption of Cm(III) and Eu(III) onto Clay Minerals under Saline Conditions: Batch Adsorption, Laser-Fluorescence Spectroscopy and Modeling. *Geochimica et Cosmochimica Acta* **2015**, *151*, 192–202. https://doi.org/10.1016/j.gca.2014.11.011.
(45) Bradbury, M. H.; Baeyens, B. Sorption Modelling on Illite Part I: Titration Measurements and the Sorption of Ni, Co, Eu and Sn. *Geochimica et Cosmochimica Acta* **2009**, *73* (4), 990–1003. https://doi.org/10.1016/j.gca.2008.11.017.

(46) Parkhurst, D. L.; Appelo, C. A. J. User's Guide to PHREEQC (Version 2): A Computer Program for Speciation, Batch-Reaction, One-Dimensional Transport, and Inverse Geochemical Calculations. *Water-resources investigations report* **1999**, *99* (4259), 312.
(47) Luo; Byrne, R. H. Yttrium and Rare Earth Element Complexation by Chloride Ions at 25°C. *Journal of Solution Chemistry* **2001**, *30* (9), 837–845. https://doi.org/10.1023/A:1012292417793.
(48) Klungness, G. D.; Byrne, R. H. Comparative Hydrolysis Behavior of the Rare Earths and Yttrium: The Influence of Temperature and Ionic Strength. *Polyhedron* **2000**, *19* (1), 99–107. https://doi.org/10.1016/S0277-5387(99)00332-0.
(49) Luo, Y.-R.; Byrne, R. H. Carbonate Complexation of Yttrium and the Rare Earth Elements in Natural Waters. *Geochimica et Cosmochimica Acta* **2004**, *68* (4), 691–699. https://doi.org/10.1016/S0016-7037(03)00495-2.
(50) Diakonov, I. I.; Ragnarsdottir, K. V.; Tagirov, B. R. Standard Thermodynamic Properties and Heat Capacity Equations of Rare Earth Hydroxides: *Chemical Geology* **1998**, *151* (1–4), 327–347. https://doi.org/10.1016/S0009-2541(98)00088-6.
(51) NEA. *Second Update on the Chemical Thermodynamics of Uranium, Neptunium, Plutonium, Americium and Technetium*; OECD Publishing, Paris, 2020; Vol. 14.
(52) NEA. *Chemical Thermodynamics of Thorium*; Chemical Thermodynamics; OECD Publishing, Paris, 2009. https://doi.org/10.1787/9789264056688-en.
(53) Brown, P. L.; Ekberg, C. *Hydrolysis of Metal Ions*; John Wiley & Sons, 2016.
(54) Marsac, R.; Martin, S.; Boily, J.-F.; Hanna, K. Oxolinic Acid Binding at Goethite and Akaganéite Surfaces: Experimental Study and Modeling. *Environ. Sci. Technol.* **2016**, *50* (2), 660–668. https://doi.org/10.1021/acs.est.5b04940.
(55) Filius, J. D.; Hiemstra, T.; Van Riemsdijk, W. H. Adsorption of Small Weak Organic Acids on Goethite: Modeling of Mechanisms. *Journal of Colloid and Interface Science* **1997**, *195* (2), 368–380. https://doi.org/10.1006/jcis.1997.5152.
(56) Bolt, G. H. Analysis of the Validity of the Gouy-Chapman Theory of the Electric Double Layer. *Journal of Colloid Science* **1955**, *10* (2), 206–218. https://doi.org/10.1016/0095-8522(55)90027-1.
(57) Satpathy, A.; Wang, Q.; Giammar, D. E.; Wang, Z. Intercomparison and Refinement of Surface Complexation Models for U(VI) Adsorption onto Goethite Based on a Metadata Analysis. *Environmental Science & Technology* **2021**, *55* (13), 9352–9361. https://doi.org/10.1021/acs.est.0c07491.
(58) Ulrich, K.-U.; Rossberg, A.; Foerstendorf, H.; Zänker, H.; Scheinost, A. C. Molecular Characterization of Uranium(VI) Sorption Complexes on Iron(III)-Rich Acid Mine Water Colloids. *Geochimica et Cosmochimica Acta* **2006**, *70* (22), 5469–5487. https://doi.org/10.1016/j.gca.2006.08.031.
(59) Bargar, J. R.; Reitmeyer, R.; Davis, J. A. Spectroscopic Confirmation of Uranium(VI)−Carbonato Adsorption Complexes on Hematite. *Environ. Sci. Technol.* **1999**, *33* (14), 2481–2484. https://doi.org/10.1021/es990048g.
(60) Kinniburgh, D. G.; Cooper, D. M. PhreePlot: Creating Graphical Output with PHREEQC, 2011. https://phreeplot.org/.
(61) Powell, M. A Method for Minimizing a Sum of Squares of Non-Linear Functions without Calculating Derivatives. *The Computer Journal* **1965**, *7* (4), 303–307.
(62) Xu, J.; Marsac, R.; Wei, C.; Wu, F.; Boily, J.-F.; Hanna, K. Co-Binding of Pharmaceutical Compounds at Mineral Surfaces: Mechanistic Modeling of Binding and Cobinding of

Nalidixic Acid and Niflumic Acid at Goethite Surfaces. *Environmental Science & Technology* **2017**, *51* (20), 11617–11624. https://doi.org/10.1021/acs.est.7b02900.
(63) Luo, T.; Xu, J.; Cheng, W.; Zhou, L.; Marsac, R.; Wu, F.; Boily, J.-F.; Hanna, K. Interactions of Anti-Inflammatory and Antibiotic Drugs at Mineral Surfaces Can Control Environmental Fate and Transport. *Environmental Science & Technology* **2022**, *56* (4), 2378–2385. https://doi.org/10.1021/acs.est.1c06449.
(64) Pepper, S. E.; Hull, L. C.; Bottenus, B. N.; Clark, S. B. Adsorption of Lanthanum to Goethite in the Presence of Gluconate. *Radiochimica Acta* **2006**, *94* (4), 229–237. https://doi.org/10.1524/ract.2006.94.4.229.
(65) Rabung, T.; Geckeis, H.; Kim, J.-I.; Beck, H. P. Sorption of Eu(III) on a Natural Hematite: Application of a Surface Complexation Model. *Journal of Colloid and Interface Science* **1998**, *208* (1), 153–161. https://doi.org/10.1006/jcis.1998.5788.
(66) Schnurr, A.; Marsac, R.; Rabung, T.; Lützenkirchen, J.; Geckeis, H. Sorption of Cm(III) and Eu(III) onto Clay Minerals under Saline Conditions: Batch Adsorption, Laser-Fluorescence Spectroscopy and Modeling. *Geochimica et Cosmochimica Acta* **2015**, *151*, 192–202. https://doi.org/10.1016/j.gca.2014.11.011.
(67) Shannon, R. D. Revised Effective Ionic Radii and Systematic Studies of Interatomie Distances in Halides and Chaleogenides. **1976**, No. Acta Cryst. (1976). A32, 751. https://doi.org/10.1107/S0567739476001551.
(68) Ohta, A.; Kawabe, I. Rare Earth Element Partitioning between Fe Oxyhydroxide Precipitates and Aqueous NaCl Solutions Doped with NaHCO3: Determinations of Rare Earth Element Complexation Constants with Carbonate Ions. *Geochem. J.* **2000**, *34* (6), 439–454. https://doi.org/10.2343/geochemj.34.439.
(69) Tanaka, K.; Takahashi, Y.; Shimizu, H. Local Structure of Y and Ho in Calcite and Its Relevance to Y Fractionation from Ho in Partitioning between Calcite and Aqueous Solution. *Chemical Geology* **2008**, *248* (1), 104–113. https://doi.org/10.1016/j.chemgeo.2007.11.003.
(70) Ratié, G.; Zhang, K.; Iqbal, M.; Vantelon, D.; Mahé, F.; Rivard, C.; Komárek, M.; Bouhnik-Le Coz, M.; Dia, A.; Hanna, K.; Davranche, M.; Marsac, R. Driving Forces of Ce(III) Oxidation to Ce(IV) onto Goethite. *Chemical Geology* **2023**, 121547. https://doi.org/10.1016/j.chemgeo.2023.121547.
(71) Nakada, R.; Takahashi, Y.; Tanimizu, M. Isotopic and Speciation Study on Cerium during Its Solid–Water Distribution with Implication for Ce Stable Isotope as a Paleo-Redox Proxy. *Geochimica et Cosmochimica Acta* **2013**, *103*, 49–62. https://doi.org/10.1016/j.gca.2012.10.045.
(72) Powell, B. A.; Dai, Z.; Zavarin, M.; Zhao, P.; Kersting, A. B. Stabilization of Plutonium Nano-Colloids by Epitaxial Distortion on Mineral Surfaces. *Environmental Science and Technology* **2011**, *45* (7), 2698–2703. https://doi.org/10.1021/es1033487.
(73) Marsac, R.; Banik, N. L.; Lützenkirchen, J.; Buda, R. A.; Kratz, J. V.; Marquardt, C. M. Modeling Plutonium Sorption to Kaolinite: Accounting for Redox Equilibria and the Stability of Surface Species. *Chemical Geology* **2015**, *400*, 1–10. https://doi.org/10.1016/j.chemgeo.2015.02.006.
(74) Marsac, R.; Banik, N. L.; Lützenkirchen, J.; Diascorn, A.; Bender, K.; Marquardt, C. M.; Geckeis, H. Sorption and Redox Speciation of Plutonium at the Illite Surface under Highly Saline Conditions. *Journal of Colloid and Interface Science* **2017**, *485*, 59–64. https://doi.org/10.1016/j.jcis.2016.09.013.

(75) Banik, N. L.; Marsac, R.; Lützenkirchen, J.; Diascorn, A.; Bender, K.; Marquardt, C. M.; Geckeis, H. Sorption and Redox Speciation of Plutonium at the Illite Surface. *Environ. Sci. Technol.* **2016**, *50* (4), 2092–2098. https://doi.org/10.1021/acs.est.5b05129.
(76) Marsac, R.; Catrouillet, C.; Pédrot, M.; Benedetti, M. F.; Dia, A.; van Hullebusch, E. D.; Davranche, M.; Sivry, Y.; Pierson-Wickmann, A.-C.; Tharaud, M.; Heberling, F. Equilibrium Surface Complexation Modeling with Metastable Natural Colloids: The Key to Predict the Oxidation State Distribution of Trace Elements? *Current Opinion in Colloid & Interface Science* **2024**, *72*, 101820. https://doi.org/10.1016/j.cocis.2024.101820.
(77) Reiller, P.; Moulin, V.; Casanova, F.; Dautel, C. On the Study of Th(IV)-Humic Acid Interactions by Competition Sorption Studies with Silica and Determination of Global Interaction Constants. *Radiochimica Acta* **2003**, *91* (9), 513–524. https://doi.org/10.1524/ract.91.9.513.20000.
(78) Qin, H.-B.; Yang, S.; Tanaka, M.; Sanematsu, K.; Arcilla, C.; Takahashi, Y. Scandium Immobilization by Goethite: Surface Adsorption versus Structural Incorporation. *Geochimica et Cosmochimica Acta* **2021**, *294*, 255–272. https://doi.org/10.1016/j.gca.2020.11.020.
(79) Choppin, G. R.; Rao, L. F. Complexation of Pentavalent and Hexavalent Actinides by Fluoride. *Radiochimica Acta* **1984**, *37* (3), 143–146. https://doi.org/10.1524/ract.1984.37.3.143.
(80) Hsi, D.; Langmuir, D. Adsorption of Uranyl onto Ferric Oxyhydroxides: Application of the Surface Complexation Site-Binding Model. *Geochimica et Cosmochimica Acta* **1985**, *49* (9), 1931–1941. https://doi.org/10.1016/0016-7037(85)90088-2.
(81) Waite, T. D.; Davis, J. A.; Payne, T. E.; Waychunas, G. A.; Xu, N. Uranium(VI) Adsorption to Ferrihydrite: Application of a Surface Complexation Model. *Geochimica et Cosmochimica Acta* **1994**, *58* (24), 5465–5478. https://doi.org/10.1016/0016-7037(94)90243-7.
(82) Davis, J. A.; Meece, D. E.; Kohler, M.; Curtis, G. P. Approaches to Surface Complexation Modeling of Uranium(VI) Adsorption on Aquifer Sediments1 1Associate Editor: J. Rustad. *Geochimica et Cosmochimica Acta* **2004**, *68* (18), 3621–3641. https://doi.org/10.1016/j.gca.2004.03.003.
(83) Fairhurst, A. J.; Warwick, P. The Influence of Humic Acid on Europium–Mineral Interactions. *Colloids and Surfaces A: Physicochemical and Engineering Aspects* **1998**, *145* (1), 229–234. https://doi.org/10.1016/S0927-7757(98)00662-1.
(84) Naveau, A.; Monteil-Rivera, F.; Dumonceau, J.; Boudesocque, S. Sorption of Europium on a Goethite Surface: Influence of Background Electrolyte. *Journal of Contaminant Hydrology* **2005**, *77* (1–2), 1–16. https://doi.org/10.1016/j.jconhyd.2004.10.002.
(85) Armstrong, C. R.; Wood, S. A. Effect of Fulvic Acid on Neodymium Uptake by Goethite. *Journal of Colloid and Interface Science* **2012**, *387* (1), 228–233. https://doi.org/10.1016/j.jcis.2012.07.060.